1   ***Alexandrium* on the Alaskan Beaufort Sea Shelf: Impact of upwelling in a warming Arctic**

2

3   Sveinn V. Einarsson[1][β] (ORCID: 0000-0003-4057-5266; seinarsson@ufl.edu)

4   Kate Lowry[2,3]

5   Peigen Lin[3]

6   Robert S. Pickart[3]

7   Carin J. Ashjian[3]

8   P. Dreux Chappell[1][*] (ORCID: 0000-0001-5212-6228; pdchappe@odu.edu)

9

10   [1]Old Dominion University, Dept. Ocean and Earth Sciences, Norfolk, VA, USA

11   [2]Science Philanthropy Alliance, Palo Alto, CA, USA

12   [3]Woods Hole Oceanographic Institution, Woods Hole, MA, USA

13

14   [*]Corresponding author

15

16

17

[β] Present address: University of Florida Dept Microbiology and Cell Science, USDA ARS affiliate, Gainesville, FL, USA

Abstract:

The harmful algal genus *Alexandrium* has characteristically been found in temperate and subtropical regions; however recent evidence suggests global warming may be expanding its range into high latitude waters. *Alexandrium* cysts have previously been documented in the Chukchi Sea and we hypothesize that *Alexandrium* may be expanding further into the Arctic due to distribution by the Beaufort shelfbreak jet. Here we document the presence of *Alexandrium catenella* along the Alaskan Beaufort Sea shelf, marking an expansion of its known range. The observations of *A. catenella* were made using three different methods: FlowCAM imaging, 18S eukaryotic sequencing, and real-time quantitative PCR. Four occupations of a shelf/slope transect spanned the evolution of a strong wind-driven upwelling event over a 5-day period. A nearby mooring provided the physical context for the event, revealing that enhanced easterly winds reversed the Beaufort shelfbreak jet to the west and induced upwelling of colder, denser water onto the outer shelf. *A. catenella* sequences dominated the surface phytoplankton community at the onset of the upwelling event. This signal vanished during and after the event, likely due to a combination of alongstream advection, cross-stream advection, and wind mixing. These results suggest contrasting physical processes that are both subject to global warming amplification, delivery of warm waters via the Beaufort shelfbreak jet and upwelling, may control the proliferation of this potential harmful alga into the Arctic.

36 **Keywords:**

38   **1 Introduction**

39   Harmful algal blooms (HABs) have become an increasingly important issue for public

40   health. Although a recent study concluded that it was additional monitoring and awareness rather

41   than a global increase in HABs that led to more documented instances of HABs and related

42   illnesses such as paralytic shellfish poisoning (PSP) from 1985-2018 (Hallegraeff et al., 2021),

43   there is evidence for both local and regional changes amongst certain HABs, including expansion

44   of PSP into new regions associated with ocean warming (Anderson et al., 2021b). The majority

45   of human health problems associated with HABs come from the consumption of shellfish

46   (Grattan et al., 2016) with PSP accounting for a third of the shellfish illnesses (Hallegraeff et al.,

47   2021). PSP can occur when a neurotoxin, such as saxitoxin, is bioaccumulated through filter

48   feeders and fish (Cusick and Sayler, 2013; Wang, 2008), and is subsequently consumed. Certain

49   species of dinoflagellates are associated with saxitoxin production and PSP outbreaks, making

50   them a consistent concern for public health and coastal ecosystem services (Grattan et al., 2016;

51   Hallegraeff et al., 2021). The *Alexandrium* genus is one of the dinoflagellate genera that has been

52   found to be the causative agent of many instances of shellfish poisoning along the coastal United

53   States (Anderson et al., 2008; Anderson et al., 2021b; Lewitus et al., 2012). The species

54   *Alexandrium catenella*, which is a well-studied member of the genus known for its ability to

55   produce saxitoxin and causing PSP outbreaks (John et al., 2014), is of particular focus for this

56   study due to recent documented expansion into the Arctic Ocean (Anderson et al., 2021a). While

57   the *Alexandrium* genus is now a globally abundant dinoflagellate, until 1970, the *Alexandrium*

58   *tamarense* species complex (which includes *A. catenella*) was only found in Europe, North

59   America, and Japan – although it is still characteristically found in temperate and subtropical

60   regions (Lilly et al., 2007). It is important to note that the accepted nomenclature of the *A.*

61   *tamarense* species complex was recently changed to: Group 1: *A. catenella,* Group 2: *A.*

62   *mediterraneum,* Group 3: *A. tamarense,* Group 4: *A. pacificum,* and Group 5: *A. austaliense*

63   (Fraga et al., 2015; John et al., 2014; Prud'homme van Reine, 2017). As prior studies have used

64   older nomenclature customs, clarification is provided throughout this manuscript where

65   appropriate.

66   The Arctic Ocean has been warming faster than any other place on Earth, resulting in

67   more extensive sea ice retreat each year (Holland and Bitz, 2003; Manabe and Stouffer, 1980). It

68   is predicted that the Arctic will continue to warm because of enhanced ocean current heat

69   transport (Marshall et al., 2014; Marshall et al., 2015) combined with Arctic amplification (Kim

70   et al., 2016). Heat transport through the Bering Strait has increased significantly over the past

71   three decades (Woodgate, 2018) and is forecast to be one of the most influential continued

72   imports of heat to the Arctic (van der Linden et al., 2019). The inflow through the Bering Strait

73   is of particular interest to this study because it brings Pacific summer water to the Alaskan

74   Beaufort Sea shelf. This warm water is advected into the Alaskan Beaufort Sea via the Alaskan

75   Coastal Current which, upon exiting Barrow Canyon, forms the eastward-flowing Beaufort

76   shelfbreak jet (Nikolopoulos et al., 2009) (Fig 1). Increased heat transport in this region

77   associated with the Beaufort shelfbreak jet has the potential to expand the domain of normally

78   temperate algae into the Arctic. Of the temperate algae, expansion of *Alexandrium* further into

79   the Arctic is of particular concern as this expansion could have deleterious implications for the

80   economy and food production in remote regions of Alaska. Prior evidence of negative impacts

81   have been documented in marine mammal beaching along the Alaskan coast up to Point Barrow

82   that was associated with the presence of the *Alexandrium* toxin saxitoxin (Lefebvre et al., 2016).

83   Cyst beds of saxitoxin producing species of *Alexandrium* have also been documented as far north

84 as the Bering Sea and Chukchi Sea (Natsuike et al., 2017a; Natsuike et al., 2013) and most

85 recently seen ~100 km west of our study site in the Alaskan Beaufort Sea (Anderson et al.,

86 2021a). In addition to warming inflow into the Arctic resulting in evidence of *Alexandrium*

87 expansion (Anderson et al., 2021a; Natsuike et al., 2017a), average temperatures suitable for

88 germination and growth of *Alexandrium* (5-15 °C, (Natsuike et al., 2017b)) have been observed

89 just west of our study area in a region where *A. catenella* cyst beds have recently been

90 documented (Anderson et al., 2021a).

91   While the Beaufort shelfbreak jet may be delivering temperate algae further into the

92 Arctic, once delivered into the region phytoplankton may be influenced by other complicating

93 physical process such as wind-driven upwelling. Specifically, under intensified easterly winds

94 the Beaufort shelfbreak jet reverses to the west, followed shortly thereafter by upwelling (Pickart

95 et al., 2009). This upwelling can deliver nutrient-rich Pacific-origin winter water from the Arctic

96 basin onto the shelf (Lin et al., 2019; Pickart et al., 2011). Upwelling in the Beaufort Sea is

97 predicted to increase in strength and occurrence as a result of a warming climate (Pickart et al.,

98 2013). The upwelled nutrient-rich cold water can reach the surface euphotic zone where

99 phytoplankton and other biota have access to it, often leading to a bloom of phytoplankton and

100 subsequently to an increase in upper trophic level biomass in the Alaskan Beaufort Sea (Ashjian

101 et al., 2010). Some phytoplankton respond better than others to water column turbulence and

102 increased nutrient concentrations that are associated with upwelling events. Diatoms, for

103 example, are unicellular eukaryotic phytoplankton known to grow faster than other

104 phytoplankton in response to nutrient pulses, allowing them to bloom in upwelling environments

105 (Biller et al., 2013). By contrast, dinoflagellates are generally more suited to bloom when the

106 upper water column is stratified, such as after upwelling events when wind mixing ceases

107 (Lewitus et al., 2012). As a result of this dynamic, when upwelling begins it is common for the

108 phytoplankton community to shift to diatoms, and, when upwelling relaxes, the environment

109 becomes more favorable to dinoflagellates and diatom growth often enters a lag phase (Smayda

110 and Trainer, 2010).

111 Motivated by a desire to explore how these two competing physical factors, warm water

112 intrusion via the Beaufort shelfbreak jet and upwelling, may be influencing *Alexandrium*

113 populations in the coastal Arctic, this study uses multiple methods to evaluate *Alexandrium* in

114 the Beaufort shelf region at the onset, during, and after an upwelling event. We hypothesize that

115 the Beaufort shelfbreak jet is transporting warm water suitable for *Alexandrium* growth and

116 expanding its habitable region. We further hypothesize that increased upwelling can mitigate this

117 expansion of *Alexandrium* by displacing these warmer waters in addition to increasing

118 turbulence. Using data from a FlowCam imaging system, we show evidence of *Alexandrium*

119 further into the eastern Pacific Arctic domain than has been previously observed. The species of

120 *Alexandrium* was subsequently determined to be *A. catenella* using both an 18S rRNA

121 sequencing method and a 28S rRNA real-time quantitative PCR method. As *A. catenella* is a

122 toxin producing species, this proliferation is of particular concern and further study of toxicity of

123 *A. catenella* in this region may be warranted.

124 **2 Material and methods**

125 **2.1 Physical data collection**

126 A research cruise on R/V *Sikuliaq* took place in August-September 2017 as part of a program

127 investigating upwelling in the western Beaufort Sea. During the cruise, a shelf-slope transect

128 near 151°W was occupied four times between 30 August and 5 September (Fig. 1). An additional

129 test station was sampled at 71.77°N 153.34°W and is included here. Conductivity-temperature-

130 depth (CTD) stations were carried out using a Sea-Bird Electronics SBE 911-plus (Bellevue,

131 WA, USA) with dual temperature and conductivity sensors, as well as a dissolved oxygen sensor

132 (Sea-Bird SBE43) and a fluorometer (Wetlabs FLRTD). The stations were spaced ≤5 km apart,

133 and each occupation of the transect took between 10 and 18 h to complete. The transect was

134 located near a long-term mooring deployed as part of the Arctic Observing Network (AON) (Lin

135 et al., 2019). The mooring is situated at the 147 m isobath in the core of the Beaufort shelfbreak

136 jet, roughly 35 km west of the transect (Fig. 1). Velocity was measured hourly from the mooring

137 throughout the *Sikuliaq* cruise using an upward-facing Nortek Signature 250 kHz acoustic

138 Doppler current profiler (ADCP) with 4 m bins, and temperature and conductivity (salinity) were

139 measured hourly using 8 SBE MicroCATs (Sea-Bird) spaced through the water column from 33

140 m to near the seafloor. Wind data at 9.4 m height were obtained from the meteorological station

141 in Utqiaġvik, AK (Fig. 1), and 10-m wind and sea-level pressure fields from the ERA5 reanalysis

142 (Hersbach et al., 2018) were used as well. We consider the alongcoast wind (105°T, positive out

143 of west), and the alongstream velocity (125°T, positive to the east) (Lin et al., 2019;

144 Nikolopoulos et al., 2009).

145 **2.2 Sample collection**

146   Near-surface water and water from the depth of the chlorophyll *a* maximum were collected

147 using Niskin bottles on the CTD rosette. Up to 4L of seawater were drawn into 10% HCl acid-

148 cleaned and seawater-rinsed Nalgene bottles (ThermoFisher Scientific; Waltham, MA, USA), then

149 subsequently filtered through a 0.22 μm Sterivex filter (Millipore Sigma, Merck KGaA;

150 Darmstadt, Germany) using a peristaltic pump. Filters were immediately frozen at -80°C until

151 DNA extraction. Seawater was also pre-filtered through a 100 μm Nitex mesh, and 5mL of filtered

152   seawater was run at 40x (300 μm) and 100x (100 μm) magnification on the FlowCAM (Yokogawa

153   Fluid Imaging Technologies; Scarborough, ME, USA). Nitrate profiles were collected at 7 to 10

154   stations per transect occupation with an optical nitrate sensor (SUNA V2, Sea-Bird) powered with

155   an external 51 Ah battery pack. To create depth profiles, we aligned the SUNA and CTD data by

156   recorded time. Water samples from 4-6 depths at 12 stations selected from the broader cruise

157   sampling efforts, which also included additional transects along the Beaufort Sea shelf not

158   presented here, were taken for direct nitrate concentration measurements to calibrate the nitrate

159   sensor. Nitrate concentrations in those water samples were measured using an Alpkem RFA

160   continuous flow analyzer following standard colorimetric protocols (Gordon, 1993). SUNA nitrate

161   profiles were calibrated by fitting a linear regression to direct measurements from corresponding

162   depths. While additional nutrients including phosphate and silicic acid were measured from the

163   broader cruise samples used to calibrate the SUNA sensor, only a few of the stations from this

164   manuscript were part of the calibration set. Because of this, only calibrated SUNA nitrate data are

165   presented here.

166   **2.3 DNA extraction**

167   An ethanol cleaned PVC pipe cutter was used to open the 0.22 μm Sterivex (Millipore

168   Sigma) filters and an autoclaved scalpel used to remove the filter. Each filter was added to a 2

169   mL tube containing AP1 Buffer (Qiagen; Hilden, Germany) and silicon beads of 0.1- and 0.5-

170   mm size. Bead beating was done using a bead beating attachment on a Vortex-Genie® 2 and

171   vortexing at maximum speed (3200 RPM) for ~2 minutes and DNA was extracted using the

172   DNeasy Plant Mini Kit (Qiagen) following the manufacturer's protocol.

173   **2.4 DNA amplification and sequencing analysis**

174   To analyze for eukaryotic community composition, the SSU rRNA 18S V9 marker gene

175   was amplified from DNA by PCR in triplicate using 1x master mix (Phusion HF Mastermix,

176   ThermoFisher) and primers used in the Earth Microbiome Project's standard 18S Illumina

177   Sequencing protocol (Stoeck et al., 2010) on a SimpliAmp thermal cycler (Applied Biosystems;

178   Waltham, MA, USA). Triplicate PCR products were pooled, and the amplified DNA was

179   purified using Mag-Beads (AMPure XP, Beckman Coulter; Indianapolis, Indiana, USA). The

180   amplified DNA was then subject to another round of PCR, to attach MiSeq indices (Illumina;

181   San Diego, CA, USA), and Mag-Bead purified again. Sequencing was done using the Illumina

182   MiSeq Desktop Sequencer at Old Dominion University (Norfolk, Virginia, USA) using a 2×300-

183   bp kit. Sequences were analyzed by pipeline analysis using DADA2 (Callahan et al., 2016), with

184   minor exceptions to the default analysis. Reads without primer sequences were discarded from

185   analysis while intact sequences had primers removed using cutadapt (Martin 2011). Average

186   reads per sample were 66000, and Amplicon Sequence Variants (ASVs) were identified using

187   the BLASTN (Altschul et al., 1990) algorithm to an in-house database including 18S rRNA

188   eukaryote sequences from the National Center for Biotechnology and Information (NCBI;

189   Bethesda, MD, USA) and eukaryotic sequences from SILVA (the German Network for

190   Bioinformatics Infrastructure; Bremen, Germany). To calculate the 18S rRNA *A. catenella*

191   relative abundance of phytoplankton, the read counts for 4 ASVs for *A. catenella* (>99% similar)

192   were combined and divided by the combined read counts for to all 18S rRNA phytoplankton hits

193   (which includes ASVs classified as diatoms, dinoflagellates, and haptophytes). We chose to

194   calculate relative abundance of *A. catenella* in acknowledgement of the compositional nature of

195   high-throughput amplicon sequencing datasets (Gloor et al., 2017).

196   **2.5 qPCR assay**

197   Quantification of the dinoflagellates *A. catenella* and *Alexandrium pacificum* was done in

198   triplicate on a StepOne Plus real-time PCR system (ThermoFisher) using the species specific 28S

199   rRNA qPCR assays of Hosoi-Tanabe and Sako (2005) with 1x TaqMan Fast Advanced Master

200   Mix (ThermoFisher). We note that Hosoi-Tanabe and Sako used the older nomenclature and

201   refer to *A. catenella* as *A. tamarense* and *A. pacificum* as *A. catenella.* Absolute 28S rRNA gene

202   quantification was done using standard curves created by serial dilution of synthetic plasmids

203   (GENEWIZ; South Plainfield, NJ, USA) for both *A. pacificum* (previously *A. catenella)* and *A.*

204   *catenella* (previously *A. tamarense*) although *A. pacificum* was never detected in our samples

205   and will not be discussed further. *A. catenella* qPCR efficiency was 89% and standards ranged

206   from 55 to 5.5E8 gc/µl.

207   **2.6 Statistical analysis**

208   Significant difference between groups of samples was determined using a Kruskal-Wallis

209   (Kruskal and Wallis, 1952) test. This was done by comparing grouped samples collected on the

210   shelf (excluding station 2.2) at the surface and chl-*a* depths for the 4 occupations, the onset (A),

211   during (B), and after (C, D) upwelling. The Kruskal-Wallis test was chosen due to a few samples

212   being below detection limit, causing group sample counts to be uneven, and the non-normal

213   distribution of residuals for the one-way ANOVA. Significant differences between individual

214   groups was done using Dunn's post hoc test. Significance is reported with a p-value below the α

215   criterion of 0.05. A linear regression analysis was used to compare log transformed *A. catenella*

216   18S rRNA relative sequence abundance and 28S rRNA absolute sequence abundance. This

217   correlation was checked to determine if the changes in absolute and relative abundance of *A.*

218   *catenella* corroborated each other to support our argument that *A. catenella* sequence abundance

219   was higher before upwelling. Additionally, a linear regression analysis compared the log

220 transformed *A. catenella* 28S rRNA sequence abundance and CTD fluorescence when *A.*

221 *catenella* 18S rRNA sequences accounted for more than 5% of the relative phytoplankton 18S

222 rRNA sequences. This analysis was done to compare fluorescence, absolute and relative

223 sequence abundance to add support to the argument that *A. catenella* was a primary

224 phytoplankton in the community before upwelling. Strength of relationship is reported as ρ and

225 significance is reported with a p-value below the α criterion of 0.05.

226 **3 Results**

227 **3.1 Hydrography**

228 The transect was occupied four times (A, B, C, D) at different stages of a wind-driven

229 upwelling event and the physical context for the event is provided by the meteorological

230 information together with the AON mooring data (Fig. 2). Alongcoast wind velocity from ERA5

231 and the Utqiaġvik weather station is shown in the top panel (Fig. 2A). Water column

232 alongstream velocity, salinity, and potential temperature and density (referenced to the sea

233 surface) are shown in subsequent panels (Fig. 2B-D), covering the full progression of the

234 upwelling event. As the first transect was occupied, the alongcoast winds became upwelling

235 favorable. Subsequent to this, the salinity in the lower part of the water column increased and the

236 Beaufort shelfbreak jet reversed to the west. The second transect was carried out shortly after the

237 peak of the event, while the third occupation occurred after the upwelling had subsided and the

238 eastward-flowing Beaufort shelfbreak jet had become re-established. The fourth occupation took

239 place as a second, considerably weaker, upwelling event commenced.

240 The evolution of the large-scale wind and sea-level pressure (SLP) field is shown in

241 Suppl. Fig. 1. Before the first upwelling event, the winds were northerly in the study region

242 associated with the eastern side of the atmospheric Beaufort High. During the upwelling event,

243 the Beaufort High had weakened, but a low-pressure system over Alaska led to a strong zonal

244 SLP gradient over the southern Beaufort Sea. After the event, high SLP was established over

245 Alaska weakening the zonal gradient in the study region, resulting in light easterly winds.

246   The vertical sections of temperature and density (Fig. 3) and nitrate (Suppl. Fig. 2) of the

247 sampled transects reveal differences throughout the water column between the onset of the

248 primary upwelling event and the subsequent three occupations during/after the event that

249 generally agree with AON mooring data.

250 **3.2 *Alexandrium catenella* assessment**

251   FlowCAM samples taken during occupation A at the onset of upwelling imaged

252 relatively high levels of *Alexandrium* on the Beaufort Sea shelf (Suppl. Table 1, Suppl. Fig. 4)

253 and coincided with the highest absolute and relative gene abundances (Fig. 3, Suppl. Table 1,

254 Suppl. Fig. 4). Based on the absolute 28S rRNA gene abundances of *A. catenella* along with the

255 ratio of *A. catenella* 18S rRNA sequences to total 18S rRNA eukaryotic phytoplankton

256 sequences (diatoms, dinoflagellates, haptophytes), the threshold for being imaged by the

257 FlowCAM was an absolute 28S rRNA gene abundance of $> 3.92E+09$ gc L^{-1} and a relative *A.*

258 *catenella* 18S rRNA abundance of the total phytoplankton community of $> 45\%$ (Suppl. Table

259 1).

260   Grouping by occupation and averaging the surface and chl-*a* max samples, the 28S rRNA

261 absolute gene abundance were found to be significantly different using a Kruskal-Wallis test

262 (F=14.65, p=0.0021). Dunn's post hoc test comparing the groups individually (Table 1) found

263 occupation A to be significantly different than occupations B, C, and D. While no significant

264 different was seen between occupations B, C, and D. The same pattern of results was seen with

265 the relative abundance of *A. catenella,* where a significant difference was found between the

266 occupations (F = 18.57, p=0.0003). The only difference being that between occupations B and D

267 there was a significant difference (Table 2)

268   The 18S rRNA relative abundance of *A. catenella* sequencing reads to phytoplankton

269 sequencing reads is plotted against the absolute 28S rRNA gene abundance of *A. catenella* (gc L$^-$

270 ^{1}) with both on a log scale (Fig. 4A). A linear regression showed a significant correlation (r^2 =

271 0.87, p < 0.0001) between absolute gene abundance and relative abundance of *A. catenella*. The

272 relationship between absolute 28S rRNA gene abundance of *A. catenella* (when *A. catenella* was

273 above 5% of the relative 18S rRNA phytoplankton community) and fluorescence (mg m^{-3})

274 measured by the CTD (Fig. 4B) also showed a significant correlation (r^2 = 0.75, p-value =

275 0.0006). When the *A. catenella* was below 5% of the 18S rRNA phytoplankton community, no

276 such relationship exists, suggesting that *A. catenella* was likely a primary phytoplankton in the

277 community before upwelling. Absolute gene abundance of *A. pacificum* was not found in any of

278 the samples and consequently is not included in Supplemental table 1 or discussed further.

279 **4 Discussion**

280 **4.1 Hydrographic context of upwelling/relaxation states during sampling**

281   The study analyzed *A. catenella* abundances through four stages of upwelling at the same

282 location. As earlier studies have demonstrated that the alongcoast winds are most effective at

283 driving upwelling (Nikolopoulos et al., 2009), we use that metric and data from a AON mooring

284 to provide context for our transect sampling. Prior to the first occupation (A), the alongcoast

285 winds were weakly out of the west, and the Beaufort shelfbreak jet was flowing eastward. As the

286   first section was being occupied, the winds were building out of the east and the Beaufort

287   shelfbreak jet was in the process of reversing. Typically upwelling commences roughly half a

288   day after the Beaufort shelfbreak jet reverses (Pickart et al., 2009), but in this case the upwelling

289   was beginning at the same time as the flow switched directions, as indicated by the uplifting of

290   the isopycnals. The reason for this may be that a strong upwelling event in the region took place

291   from 27-29 August (not shown), and the isopycnals had not fully relaxed prior to the main

292   upwelling event considered here. As such, we refer to the first occupation as "onset of

293   upwelling."

294   The second occupation (B) took place roughly a day after the peak easterly winds, at

295   which point the isopycnals were close to their maximum elevation but beginning to relax. The

296   upper part (shallower than 80m) of the Beaufort shelfbreak jet remained reversed, while the

297   deeper part was starting to become re-established to the east, which is the typical sequence (Lin

298   et al., 2019). This crossing is referred to as "during upwelling." The third occupation (C)

299   occurred when the bulk of the Beaufort shelfbreak jet was again flowing eastward and the denser

300   isopycnals had descended significantly deeper, which corresponds to "after upwelling." The final

301   occupation (D) of the section was done during the start of another upwelling event that was

302   considerably shorter and weaker. When considered in the context of the primary event, this

303   occupation is also referred to as "after upwelling."

304   The profile data from our transects revealed that, as the event was beginning and the

305   Beaufort shelfbreak jet was switching directions (occupation A), weakly stratified warm water

306   was present over the outer shelf. This consisted mainly of Alaskan Coastal Water (>4°C) with a

307   layer of sea-ice melt water occupying the top 10 m. Seaward of the shelf, the cold halocline,

308   centered at the 26.5 kg m^{-3} isopycnal, was at its deepest depth of the four transect occupations.

309 By contrast, during the next three occupations the warm water on the shelf was largely displaced.

310 In particular, the signature of Alaskan Coastal Water nearly disappeared at the surface, replaced

311 by a thicker layer of sea-ice melt water (roughly 25 m thick) and a deep layer of colder, denser

312 Bering Summer Water along the bottom of the outer shelf. The stratification in the upper 50 m

313 became enhanced, which is consistent with past mooring results (Lin et al., 2019). Furthermore,

314 seaward of the shelf the halocline shoaled and became colder. We note, however, that the denser

315 27.0 and 27.5 kg m^{-3} isopycnals were at their shallowest depth during occupation B, consistent

316 with the AON mooring data indicating that this was near the height of the upwelling.

4.2 *A. catenella* presence on the Beaufort Shelf

318   This study confirms the presence and abundance of *Alexandrium* – specifically the

319 species *A. catenella* – on the Alaskan Beaufort Sea shelf using imaging, sequencing, and qPCR

320 methods. It is known that dinoflagellates have higher gene copy numbers than other unicellular

321 eukaryotes (Cusick and Sayler, 2013; Lin, 2011), thus there is some concern when using

322 ribosomal gene abundance to analyze eukaryotic community composition due to this copy

323 number variability. However, we are encouraged that when *Alexandrium* was imaged by

324 FlowCAM in a sample (n=5), it corresponded with the five highest samples in terms of *A.*

325 *catenella* 18S rRNA relative abundance of phytoplankton sequences, and the five highest

326 absolute 28S rRNA gene abundances of *A. catenella*. Furthermore, our combined approach

327 found that as the relative abundance of *A. catenella,* as a proportion of phytoplankton sequences,

328 increased, the absolute gene abundance of *A. catenella* in our samples increased. Based on our

329 results, the thresholds for visualization on the FlowCAM were > 3.92E+09 gc L^{-1} for 28S rRNA

330 gene abundance, which was associated with >45% relative abundance of *A. catenella* in total 18S

331 rRNA reads. Even though we found the three methods of measuring *A. catenella* abundance to

332   corroborate with each other, because of known issues with variability in ribosomal gene

333   abundance discussed above and the small size of our dataset, we caution against using this value

334   as a hard threshold. We are encouraged, however, that with further sampling of *A. catenella*

335   using these methods it may be possible to determine with more certainty the threshold at which

336   *A. catenella* is imaged on the FlowCAM. A loftier but potentially achievable goal would be to

337   further determine a threshold associated with toxic blooms. This would potentially allow for the

338   use of imaging equipment like FlowCAM to analyze samples collected from remote areas for

339   monitoring.

340   Previous work has estimated that the average number of 18S rRNA copies per cell of *A.*

341   *catenella* is 46000 (Yarimizu et al., 2021). If we use this value to convert our results into cell

342   densities, the threshold density to be imaged on the FlowCAM was 67000 cells L^{-1}, which is an

343   order of magnitude higher than 1000 cells L^{-1} found to be the level at which *A. catenella* can

344   pose a health risk (Jester et al., 2009). We acknowledge that *A. catenella* 28S rRNA sequence

345   counts may be overestimated using this approach due to the qPCR standard curve method used

346   (Hou et al., 2010) and known variability in ribosomal copy numbers per cell depending on the

347   strain (Yarimizu et al., 2021). In addition, without knowing the level of toxin in these samples it

348   is unsure whether the abundance of *A. catenella* were at levels that could pose a health risk. That

349   said, the three methods we used validate each other and may indicate that the cell densities of *A.*

350   *catenella* were at problematic levels before upwelling was at its peak.

351   **4.3 *A. catenella* upwelling response**

352   The results show that the absolute and relative abundances of *A. catenella* were

353   statistically different at the onset of the upwelling event (occupation A) versus during/after the

354   event (occupations B, C, and D). More specifically, our qPCR results show ~2 orders of

355 magnitude higher *A. catenella* on the shelf and in the vicinity of the shelfbreak at the onset of the

356 upwelling event when compared to samples collected during and after the event. The same

357 pattern was seen in the 18S rRNA relative gene abundance of *A. catenella,* where it accounted

358 for >40% of the eukaryotic phytoplankton sequencing reads at the start of upwelling and

359 decreased to <1% after the upwelling. There was one exception to these general patterns on the

360 shelf, which is that slightly higher relative abundance of 18S rRNA and absolute abundance of

361 28S rRNA were detected in the surface sample collected at the onshore start of the transect after

362 upwelling (occupation C).

363   It is widely understood that an increase in nutrients in the euphotic zone should lead to

364 higher algal biomass (Cushing, 1971; Iles et al., 2012; Jackson et al., 2011; Loubere, 2000;

365 Tenore et al., 1995), but the abundance of *A. catenella* dramatically dropped during the

366 upwelling when increased nitrate concentrations were found on the Alaskan Beaufort Sea shelf.

367 This is consistent with evidence that dinoflagellates often dominate the phytoplankton

368 community during lag phases between upwelling events, after diatoms have responded to the

369 increase in nutrients (Lewitus et al., 2012). *Alexandrium* is thought to initiate blooms offshore

370 and accumulate in coastal areas only after upwelling favorable winds subside (Anderson et al.,

371 2008). Nitrate profile data from the calibrated SUNA sensor enabled us to confirm that nitrate

372 upwelling occurred with the shallowing of the isopycnals associated with wind shifts. It is

373 reasonable to assume that additional nutrient concentrations also increased with upwelling based

374 on previous work in the area (Eddy et al., 2004; Mundy et al., 2009). However, as additional

375 nutrients such as silicic acid and phosphate were only measured on a handful of samples from the

376 broader cruise, we are unable to comment on whether species distributions changes could have

377   been associated with specific shifts in macronutrient ratios (i.e., between nitrate, phosphate,

378   silicic acid ratios) or simply as a result of the arrival of elevated nutrients as a whole.

379   These results are supportive of our hypothesis that the *Alexandrium* population present in

380   our study site at the onset of upwelling had been transported there by the eastward-flowing

381   Beaufort shelfbreak jet. This hypothesis is also consistent with previous data collected 105 km

382   west of our study site where high levels of *Alexandrium* were measured on a transect just east of

383   Barrow Canyon occupied in August 2018-2019 (Anderson et al., 2021a). In that study the cells

384   were found in the warm Alaskan Coastal Water and sea-ice melt water being advected eastward

385   in the Beaufort shelfbreak jet and it was suggested that the cells may have entered the water

386   column from a local seed bed just east of the canyon (Anderson et al., 2021a). At the time, the

387   Barrow Canyon was the furthest east that *Alexandrium* had been observed along the northern

388   Alaskan coast. Our work indicates that the proliferation of *Alexandrium* by the Beaufort

389   shelfbreak jet continues east much further than Barrow Canyon. Further evidence that the

390   Beaufort shelfbreak jet is the main conduit for *Alexandrium* proliferation into the Beaufort Sea is

391   that the sample from the upper slope (~41 km from the onshore end of the transect and further

392   offshore than the Beaufort shelfbreak jet) showed only slightly enhanced levels of *Alexandrium*

393   at the onset of upwelling. Additionally, test station samples collected at the start of the

394   expedition in the center of the Beaufort shelfbreak jet had similarly high *A. catenella* gene counts

395   as those observed in our main transect at the onset of upwelling. The absence of both the Alaskan

396   Coastal Water and the *Alexandrium* signal during occupations B, C, and D is likely due to the

397   reversed Beaufort shelfbreak jet having advected them back to the west. Additionally, the

398   secondary circulation during the upwelling event would tend to transport material offshore in the

399   surface Ekman layer (Schulze and Pickart, 2012), which, together with enhanced wind mixing

400   during upwelling (Spall, 2004), could significantly reduce the surface signature of *Alexandrium*

401   on the shelf.

402   **4.4 A comment on numerical abundances of *A. catenella***

403   While our results found that the relative abundance of *A. catenella* at times accounted for

404   up to 45% of the phytoplankton 18S rRNA reads, it is important to note that this likely reflects

405   higher ribosomal gene counts found in dinoflagellates compared with other phytoplankton (Gong

406   and Marchetti, 2019; Lin, 2011). In other words, it would likely be an overestimation to state that

407   *A. catenella* comprised 45% of the phytoplankton community at this time. That said, in samples

408   collected at the onset of upwelling (and all samples where *A. catenella* accounted for > %5 of the

409   18S rRNA reads), fluorescence had a significant positive relationship with *A. catenella* absolute

410   gene abundance. Thus, while *A. catenella* may not have accounted for 45% of the phytoplankton

411   community, we can infer that it was likely an important part of the phytoplankton biomass at the

412   onset of the upwelling. We acknowledge that the outlier in the top right corner of Fig. 4B

413   appears to skew the regression analysis. This potential outlier was sampled at the chlorophyll

414   max depth (depth at which fluorescence was highest) at the Test Station (Fig. 1), which was

415   located roughly in the middle of the shelfbreak jet before any upwelling had occurred. Both the

416   surface and chlorophyll max samples from this station were included in this visualization and

417   analysis to further analyze the contribution *A. catenella* had to the relative phytoplankton

418   community. With the limited number of samples, we did not want to exclude any available data

419   points. Removing the possible outlier point changes the absolute value of the regression and we

420   caution that the intent of this figure is not to quantify a relationship between gc L^{-1} of *A.*

421   *catenella* and fluorescence. The point of the exercise was to confirm that when the relative

422   abundance of *A. catenella* 18S sequences accounted for a significant percentage of the

423   phytoplankton community 18S sequences, there was a corresponding increase in both 28S

424   absolute gene abundance of *A. catenella* and fluorescence, indicating that *A. catenella* was a

425   dominant component of the phytoplankton community in these samples. During and after the

426   upwelling no such relationship is seen between *A. catenella* gene abundance and fluorescence,

427   no *Alexandrium* images were observed by the FlowCAM, and there was low relative abundance

428   of *A. catenella* 18S rRNA reads. This suggests that, as the Beaufort shelfbreak jet reversed

429   during upwelling, the *A. catenella* population decreased and it was no longer a dominant

430   phytoplankton in the region.

4.5 Future monitoring

432   *A. catenella* is one of the species of the *Alexandrium* genus that forms resting cysts as a

433   part of their life cycle, and *Alexandrium* cysts are known to have an internal clock to bloom

434   when suitable conditions exist (Anderson et al., 2014). *A. catenella* cysts have been found in

435   temperature ranges from -0.6 to 26.8 °C, with the highest abundances found between 5 – 15 °C

436   (Marret and Zonneveld, 2003). The surface temperature on the shelf at the onset of the upwelling

437   event was > 5 °C. As *Alexandrium* has the ability to produce resting cysts to survive and take

438   advantage of suitable conditions (Anderson et al., 2014; Brosnahan et al., 2017; Wall, 1971), it

439   may be important to monitor this area for future *Alexandrium* blooms and further expansion

440   associated with the Beaufort shelfbreak jet. Future monitoring may be especially important

441   considering that *A. catenella* has been observed in the California Current upwelling system as an

442   opportunistic dinoflagellate that can germinate in a variety of conditions, including upwelling

443   (Pitcher et al., 2017), although our data did not show evidence of *Alexandrium* associated with

444   Arctic upwelling. The region of the shelf where *A. catenella* was observed is relatively shallow

445   (~21 m to 56 m), thus strong storms that lead to mixing events on the shelf, could resuspend

446   *Alexandrium* cysts and possibly lead to a bloom. While upwelling was seen to cause a sharp drop

447   in the abundance of *A. catenella* in our study, presumably the mixing caused by upwelling could

448   also cause a reintroduction of *A. catenella* cysts to the water column, which may lead to the

449   germination and proliferation of the cells as upwelling relaxes and warm Beaufort shelfbreak jet

450   water begins to flow on the shelf again. While in our study two competing factors were

451   documented to influence *Alexandrium* abundance, the Beaufort shelfbreak jet and

452   upwelling/reversal of the Beaufort shelfbreak jet, another factor to consider is the resuspension

453   of *A. catenella* cysts and subsequent germination during suitable periods between upwelling

454   events. As was documented by Anderson et al. (2021a) a large cyst bed of *A. catenella* is located

455   on the shelf west of our sampling site. This reinforces that more study is needed to accurately

456   document abundance and toxicity throughout this region, as the factors influencing *A. catenella*

457   abundance indicate likely prevalence and further dispersion of the HAB with periods of

458   decreased abundance during upwelling. Additional sampling in this area that includes analysis

459   of nutrients, targeted toxin testing, cell imaging, and sequencing analysis at a higher resolution

460   covering a time period fully encompassing upwelling, relaxation, and standard flow of the

461   Beaufort shelfbreak jet, will likely allow for a stronger foundation to correlate *A. catenella*

462   abundance with non-upwelling and upwelling events. Importantly, these results can be added to

463   harmful algal bloom modeling efforts to predict future occurrences of toxic levels of *A.*

464   *catenella*.

465   While not all species or even strains of *Alexandrium* produce saxitoxin (Anderson et al.,

466   2012), there have been documented cases of *Alexandrium* blooms, and saxitoxin

467   bioaccumulation, seen along the Alaskan coast up to and just east of Point Barrow (Lefebvre et

468   al., 2016). Presumably, these events were the result of the Alaskan Coastal Current bringing

469 warm water suitable for *Alexandrium* populations to thrive and they produced saxitoxin that

470 eventually led to marine mammal deaths. It has been noted that *Alexandrium* may produce

471 saxitoxin as a pheromone or as an indicator of cyst settlement (Wyatt and Jenkinson, 1997); thus,

472 if an *Alexandrium* bloom is observed in this area, saxitoxin and any further bioaccumulation will

473 need to be monitored closely. Due to the previously documented bioaccumulation of saxitoxin

474 seen along the coast of Alaska up to Point Barrow (Lefebvre et al., 2016), we can hypothesize

475 that this proliferation will continue along the Alaskan Beaufort Sea coast because of delivery by

476 the warming Beaufort shelfbreak jet, the warming Arctic as a whole, and the potential for

477 transport from the cyst beds of *Alexandrium* west of our study site. This proliferation is a

478 concern as fish, sea birds, and mammals, including bowhead and beluga whales, are known to

479 spawn in this region primarily due upwelling events that cause increased primary production and

480 zooplankton proliferation (Ashjian et al., 2010). Any proliferation of a potential toxin-producing

481 organism that can impact upper trophic levels in the region would be especially consequential to

482 the Inuvialuit, indigenous people in the western Canadian Arctic, who depend on this ecosystem

483 (Ayles et al., 2016).

484   Finding *A. catenella* this far east on the Alaskan Beaufort Sea shelf indicates that the

485 Beaufort shelfbreak jet continues transporting warm water suitable for *Alexandrium* population

486 expansion well past Barrow Canyon. It should also be noted that strong westerly winds are

487 common in this region during summer, which accelerate the Beaufort shelfbreak jet and lead to

488 downwelling (Foukal et al., 2019). This is notable, as it is similar to an anomaly that aligned with

489 an *A. catenella* (referred to as *A. fundyense* in cited study) bloom in the Gulf of Maine where

490 downwelling favorable winds were thought to have caused a coastal accumulation of

491 *Alexandrium* (McGillicuddy et al., 2014). Easterly winds in the Alaskan Beaufort Sea intensify

492   in the fall, and upwelling activity increases (Lin et al., 2016; Pickart et al., 2013). This tends to

493   slow the Beaufort shelfbreak jet, flux warm surface water offshore, and upwell colder water from

494   the basin. Indeed, Bering Summer Water replaced much of the Alaskan Coastal Water over the

495   outer shelf on occupations B-D. This upwelled water was several degrees colder, changing the

496   environmental conditions away from those likely suitable for *Alexandrium*. These results lead us

497   to suspect that if *A. catenella* were to bloom, it would occur earlier in the Arctic summer when

498   the Beaufort shelfbreak jet advects warm water to the Beaufort Sea and is not subject to as much

499   upwelling. It is worth noting, however, that there are evolutionary adaptations in *Alexandrium*

500   species that could allow for survival during upwelling, such as temporary chain formations and

501   shifts in swimming velocity to adjust to turbulence (Smayda and Trainer, 2010). These

502   evolutionary advantages suggest that increased upwelling alone may not deter *Alexandrium* from

503   surviving on the Alaskan Beaufort Sea shelf.

504   **5 Conclusion**

505   Heat transport by currents into the Arctic is predicted to continue increasing (Marshall et al.,

506   2014; Marshall et al., 2015) presumably resulting in the Beaufort shelf continuing to warm.

507   Higher temperatures in coastal waters have been determined to cause the accumulation of *A.*

508   *catenella* in the Gulf of Maine (He and McGillicuddy Jr., 2008), and, with the likely warming of

509   the Beaufort Sea shelf, we can predict that the same may occur here. However, since upwelling

510   along the Beaufort Sea shelf is predicted to increase as well (Pickart et al., 2013), there are

511   competing forces at play that could influence *Alexandrium* proliferation in the region. Either

512   way, it is prudent to further evaluate this area for *A. catenella* cell densities, toxin production and

513   determine the extent to which the Beaufort shelfbreak jet and upwelling influence levels of *A.*

514   *catenella.*

528 **Competing Interests:** The authors declare no competing interests.

529 **Data availability:** Sample and station information, including qPCR results, and nitrate profiles

530 are hosted at Arctic Data Center (https://arcticdata.io/; ID: urn:uuid:d98cfda6-7434-4201-8877-

531 163ba5708074). Cruise CTD files can be found on R2R (https://www.rvdata.us/; Cruise ID:

532 SKQ201713S) Raw sequence files can be accessed via NCBI SRA

533 (https://www.ncbi.nlm.nih.gov/sra; BioProject ID: PRJNA743005). FlowCAM images can be

534 found on Ecotaxa (https://ecotaxa.obs-vlfr.fr/; Project ID: skq201713s).

References

535

536 Altschul, S.F., Gish, W., Miller, W., Myers, E.W., Lipman, D.J., 1990. Basic local alignment
537 search tool. J. Mol. Biol. 215(3), 403-410. http://dx.doi.org/10.1016/S0022-2836(05)80360-2.

538 Anderson, D.M., Alpermann, T.J., Cembella, A.D., Collos, Y., Masseret, E., Montresor, M.,
539 2012. The globally distributed genus Alexandrium: multifaceted roles in marine ecosystems and
540 impacts on human health. Harmful Algae 14, 10-35. https://doi.org/10.1016/j.hal.2011.10.012.

541 Anderson, D.M., Burkholder, J.M., Cochlan, W.P., Glibert, P.M., Gobler, C.J., Heil, C.A.,
542 Kudela, R.M., Parsons, M.L., Rensel, J.E.J., Townsend, D.W., Trainer, V.L., Vargo, G.A., 2008.
543 Harmful algal blooms and eutrophication: Examining linkages from selected coastal regions of
544 the United States. Harmful Algae 8(1), 39-53. https://doi.org/10.1016/j.hal.2008.08.017.

545 Anderson, D.M., Fachon, E., Pickart, R.S., Lin, P., Fischer, A.D., Richlen, M.L., Uva, V.,
546 Brosnahan, M.L., McRaven, L., Bahr, F., Lefebvre, K., Grebmeier, J.M., Danielson, S.L., Lyu,
547 Y., Fukai, Y., 2021a. Evidence for massive and recurrent toxic blooms of *Alexandrium catenella*
548 in the Alaskan Arctic. PNAS 118(41), e2107387118. https://doi.org/10.1073/pnas.2107387118.

549 Anderson, D.M., Fensin, E., Gobler, C.J., Hoeglund, A.E., Hubbard, K.A., Kulis, D.M.,
550 Landsberg, J.H., Lefebvre, K.A., Provoost, P., Richlen, M.L., Smith, J.L., Solow, A.R., Trainer,
551 V.L., 2021b. Marine harmful algal blooms (HABs) in the United States: History, current status
552 and future trends. Harmful Algae 102, 101975. https://doi.org/10.1016/j.hal.2021.101975.

553 Anderson, D.M., Keafer, B.A., Kleindinst, J.L., McGillicuddy, D.J., Martin, J.L., Norton, K.,
554 Pilskaln, C.H., Smith, J.L., Sherwood, C.R., Butman, B., 2014. Alexandrium fundyense cysts in
555 the Gulf of Maine: Long-term time series of abundance and distribution, and linkages to past and
556 future blooms. Deep-Sea Res. Pt. II 103, 6-26. https://doi.org/10.1016/j.dsr2.2013.10.002.

557 Ashjian, C.J., Braund, S.R., Campbell, R.G., George, J.C.C., Kruse, J., Maslowski, W., Moore,
558 S.E., Nicolson, C.R., Okkonen, S.R., Sherr, B.F., Sherr, E.B., Spitz, Y.H., 2010. Climate
559 Variability, Oceanography, Bowhead Whale Distribution, and Inupiat Subsistence Whaling near
560 Barrow, Alaska. Arctic 63(2), 179-194. https://doi.org/10.14430/arctic973.

561 Ayles, B., Porta, L., Clarke, R.M., 2016. Development of an integrated fisheries co-management
562 framework for new and emerging commercial fisheries in the Canadian Beaufort Sea. Mar.
563 Policy 72, 246-254. https://doi.org/10.1016/j.marpol.2016.04.032.

564 Biller, D.V., Coale, T.H., Till, R.C., Smith, G.J., Bruland, K.W., 2013. Coastal iron and nitrate
565 distributions during the spring and summer upwelling season in the central California Current
566 upwelling regime. Cont. Shelf. Res. 66, 58-72. http://dx.doi.org/10.1016/j.csr.2013.07.003.

567 Brosnahan, M.L., Ralston, D.K., Fischer, A.D., Solow, A.R., Anderson, D.M., 2017. Bloom
568 termination of the toxic dinoflagellate Alexandrium catenella: Vertical migration behavior,
569 sediment infiltration, and benthic cyst yield. Limnol. Oceanogr. 62(6), 2829-2849.
570 https://doi.org/10.1002/lno.10664.

571 Callahan, B.J., McMurdie, P.J., Rosen, M.J., Han, A.W., Johnson, A.J.A., Holmes, S.P., 2016.
572 DADA2: High-resolution sample inference from Illumina amplicon data. Nat. Methods 13(7),
573 581-583. https://doi.org/10.1038/nmeth.3869.

574 Cushing, D.H., 1971. Upwelling and the Production of Fish. Adv. Mar. Biol. 9, 255-334.
575 http://dx.doi.org/10.1016/S0065-2881(08)60344-2.

576 Cusick, K.D., Sayler, G.S., 2013. An overview on the marine neurotoxin, saxitoxin: genetics,
577 molecular targets, methods of detection and ecological functions. Mar. Drugs 11(4), 991-1018.
578 https://doi.org/10.3390/md11040991.

579 Eddy, C.C., Robie, W.M., Steve, J., 2004. Phytoplankton productivity on the Canadian Shelf of
580 the Beaufort Sea. Mar. Ecol. Prog. Ser. 277, 37-50. https://doi.org/10.3354/meps277037.

581 Foukal, N.P., Pickart, R.S., Moore, G.W.K., Lin, P., 2019. Shelfbreak Downwelling in the
582 Alaskan Beaufort Sea. J. Geophys. Res-Oceans 124(10), 7201-7225.
583 https://doi.org/10.1029/2019JC015520.

584 Fraga, S., Sampedro, N., Larsen, J., Moestrup, Ø., Calado, A.J., 2015. Arguments against the
585 proposal 2302 by John & al. to reject the name Gonyaulax catenella (Alexandrium catenella).
586 Taxon 64(3), 634-635. https://doi.org/10.12705/643.15.

587 Gloor, G.B., Macklaim, J.M., Pawlowsky-Glahn, V., Egozcue, J.J., 2017. Microbiome Datasets
588 Are Compositional: And This Is Not Optional. Front. Microbiol. 8.
589 https://doi.org/10.3389/fmicb.2017.02224.

590 Gong, W., Marchetti, A., 2019. Estimation of 18S Gene Copy Number in Marine Eukaryotic
591 Plankton Using a Next-Generation Sequencing Approach. Front. Mar. Sci. 6(219).
592 https://doi.org/10.3389/fmars.2019.00219.

593 Gordon, L.I., J.C. Jennings, Jr., A.A. Ross, and J.M. Krest 1993. A suggested protocol for
594 continuous flow automated analysis of seawater nutrients (phosphate, nitrate, nitrite and silicic
595 acid) in the WOCE Hydrographic Program and the Joint Global Ocean Fluxes Study. WOCE
596 Hydrogr. Progr. Off., Methods Manual WHPO, 1-52.

597 Grattan, L.M., Holobaugh, S., Morris, J.G., 2016. Harmful algal blooms and public health.
598 Harmful Algae 57, 2-8. https://doi.org/10.1016/j.hal.2016.05.003.

599 Hallegraeff, G., Enevoldsen, H., Zingone, A., 2021. Global harmful algal bloom status reporting.
600 Harmful Algae 102(101992). https://doi.org/10.1016/j.hal.2021.101992.

601 He, R., McGillicuddy Jr., D.J., 2008. Historic 2005 toxic bloom of Alexandrium fundyense in
602 the west Gulf of Maine: 1. In situ observations of coastal hydrography and circulation. J.
603 Geophys. Res-Oceans 113(C7). https://doi.org/10.1029/2007JC004601.

604 Hersbach, H., Rosnay, P., Schepers, D., Simmons, A., Soci, C., Abdalla, S., Alonso, M.,
605 Balmaseda, Balsamo, G., Bechtold, P., Berrisford, P., Bidlot, J., Boisséson, E.D., Bonavita,
606 Browne, P., Diamantakis, M., 2018. Operational global reanalysis : progress , future directions
607 and synergies with NWP, ERA Report Series, Reading.

608 Holland, M.M., Bitz, C.M., 2003. Polar amplification of climate change in coupled models.
609 Clim. Dynam. 21(3), 221-232. https://doi.org/10.1007/s00382-003-0332-6.

610 Hosoi-Tanabe, S., Sako, Y., 2005. Species-specific detection and quantification of toxic marine
611 dinoflagellates Alexandrium tamarense and A. catenella by Real-time PCR assay. Mar
612 Biotechnol 7(5), 506-514. https://doi.org/10.1007/s10126-004-4128-4.

613 Hou, Y., Zhang, H., Miranda, L., Lin, S., 2010. Serious Overestimation in Quantitative PCR by
614 Circular (Supercoiled) Plasmid Standard: Microalgal pcna as the Model Gene. PLOS ONE 5(3),
615 e9545. https://doi.org/10.1371/journal.pone.0009545.

616 Iles, A.C., Gouhier, T.C., Menge, B.A., Stewart, J.S., Haupt, A.J., Lynch, M.C., 2012. Climate-
617 driven trends and ecological implications of event-scale upwelling in the California Current
618 System. Glob. Change Biol. 18(2), 783-796. https://doi.org/10.1111/j.1365-2486.2011.02567.x.

619 Jackson, T., Bouman, H.A., Sathyendranath, S., Devred, E., 2011. Regional-scale changes in
620 diatom distribution in the Humboldt upwelling system as revealed by remote sensing:
621 implications for fisheries. ICES J. Mar. Sci. 68(4), 729-736.
622 https://doi.org/10.1093/icesjms/fsq181.

623 Jester, R., Lefebvre, K., Langlois, G., Vigilant, V., Baugh, K., Silver, M.W., 2009. A shift in the
624 dominant toxin-producing algal species in central California alters phycotoxins in food webs.
625 Harmful Algae 8(2), 291-298. https://doi.org/10.1016/j.hal.2008.07.001.

626 John, U., Litaker, R.W., Montresor, M., Murray, S., Brosnahan, M.L., Anderson, D.M., 2014.
627 Formal revision of the Alexandrium tamarense species complex (Dinophyceae) taxonomy: the
628 introduction of five species with emphasis on molecular-based (rDNA) classification. Protist
629 165(6), 779-804. https://doi.org/10.1016/j.protis.2014.10.001.

630 Kim, K.Y., Hamlington, B.D., Na, H., Kim, J., 2016. Mechanism of seasonal Arctic sea ice
631 evolution and Arctic amplification. Cryosphere 10(5), 2191-2202. https://doi.org/10.5194/tc-10-
632 2191-2016.

633 Kruskal, W.H., Wallis, W.A., 1952. Use of Ranks in One-Criterion Variance Analysis. J. Am.
634 Stat. Assoc. 47(260), 583-621. https://doi.org/10.1080/01621459.1952.10483441.

635 Lefebvre, K.A., Quakenbush, L., Frame, E., Huntington, K.B., Sheffield, G., Stimmelmayr, R.,
636 Bryan, A., Kendrick, P., Ziel, H., Goldstein, T., Snyder, J.A., Gelatt, T., Gulland, F., Dickerson,
637 B., Gill, V., 2016. Prevalence of algal toxins in Alaskan marine mammals foraging in a changing
638 arctic and subarctic environment. Harmful Algae 55, 13-24.
639 https://doi.org/10.1016/j.hal.2016.01.007.

640 Lewitus, A.J., Horner, R.A., Caron, D.A., Garcia-Mendoza, E., Hickey, B.M., Hunter, M.,
641 Huppert, D.D., Kudela, R.M., Langlois, G.W., Largier, J.L., Lessard, E.J., RaLonde, R., Jack
642 Rensel, J.E., Strutton, P.G., Trainer, V.L., Tweddle, J.F., 2012. Harmful algal blooms along the
643 North American west coast region: History, trends, causes, and impacts. Harmful Algae 19, 133-
644 159. https://doi.org/10.1016/j.hal.2012.06.009.

645 Lilly, E.L., Halanych, K.M., Anderson, D.M., 2007. Species boundaries and global biogeography
646 of the Alexandrium tamarense complex (Dinophyceae)1. J. Phycol. 43(6), 1329-1338.
647 https://doi.org/10.1111/j.1529-8817.2007.00420.x.

648 Lin, P., Pickart, R.S., Moore, G.W.K., Spall, M.A., Hu, J., 2019. Characteristics and dynamics of
649 wind-driven upwelling in the Alaskan Beaufort Sea based on six years of mooring data. Deep-
650 Sea Res. Pt. II 162, 79-92. https://doi.org/10.1016/j.dsr2.2018.01.002.

651 Lin, P., Pickart, R.S., Stafford, K.M., Moore, G.W.K., Torres, D.J., Bahr, F., Hu, J., 2016.
652 Seasonal variation of the Beaufort shelfbreak jet and its relationship to Arctic cetacean
653 occurrence. J. Geophys. Res-Oceans 121(12), 8434-8454.
654 https://doi.org/10.1002/2016JC011890.

655 Lin, S., 2011. Genomic understanding of dinoflagellates. Res. Microbiol. 162(6), 551-569.
656 https://doi.org/10.1016/j.resmic.2011.04.006.

657 Loubere, P., 2000. Marine control of biological production in the eastern equatorial Pacific
658 Ocean. Nature 406(6795), 497-500. https://doi.org/10.1038/35020041.

659 Manabe, S., Stouffer, R.J., 1980. Sensitivity of a global climate model to an increase of CO_2
660 concentration in the atmosphere. J. Geophys. Res-Oceans 85(C10), 5529-5554.
661 https://doi.org/10.1029/JC085iC10p05529.

662 Marret, F., Zonneveld, K.A.F., 2003. Atlas of modern organic-walled dinoflagellate cyst
663 distribution. Rev. Palaeobot. Palynol. 125(1), 1-200. https://doi.org/10.1016/S0034-
664 6667(02)00229-4.

665 Marshall, J., Armour, K.C., Scott, J.R., Kostov, Y., Hausmann, U., Ferreira, D., Shepherd, T.G.,
666 Bitz, C.M., 2014. The ocean's role in polar climate change: asymmetric Arctic and Antarctic
667 responses to greenhouse gas and ozone forcing. Philos. T. R. Soc. A 372(2019), 20130040.
668 https://doi.org/10.1098/rsta.2013.0040.

669 Marshall, J., Scott, J.R., Armour, K.C., Campin, J.M., Kelley, M., Romanou, A., 2015. The
670 ocean's role in the transient response of climate to abrupt greenhouse gas forcing. Clim. Dynam.
671 44(7), 2287-2299. https://doi.org/10.1007/s00382-014-2308-0.

672 McGillicuddy, D.J., Brosnahan, M.L., Couture, D.A., He, R., Keafer, B.A., Manning, J.P.,
673 Martin, J.L., Pilskaln, C.H., Townsend, D.W., Anderson, D.M., 2014. A red tide of Alexandrium
674 fundyense in the Gulf of Maine. Deep-Sea Res. Pt. II 103, 174-184.
675 https://doi.org/10.1016/j.dsr2.2013.05.011.

676 Mundy, C.J., Gosselin, M., Ehn, J., Gratton, Y., Rossnagel, A., Barber, D.G., Martin, J.,
677 Tremblay, J.-É., Palmer, M., Arrigo, K.R., Darnis, G., Fortier, L., Else, B., Papakyriakou, T.,
678 2009. Contribution of under-ice primary production to an ice-edge upwelling phytoplankton
679 bloom in the Canadian Beaufort Sea. Geophys. Res. Lett. 36(17).
680 https://doi.org/10.1029/2009GL038837.

681 Natsuike, M., Matsuno, K., Hirawake, T., Yamaguchi, A., Nishino, S., Imai, I., 2017a. Possible
682 spreading of toxic Alexandrium tamarense blooms on the Chukchi Sea shelf with the inflow of
683 Pacific summer water due to climatic warming. Harmful Algae 61, 80-86.
684 https://doi.org/10.1016/j.hal.2016.11.019.

685 Natsuike, M., Nagai, S., Matsuno, K., Saito, R., Tsukazaki, C., Yamaguchi, A., Imai, I., 2013.
686 Abundance and distribution of toxic Alexandrium tamarense resting cysts in the sediments of the
687 Chukchi Sea and the eastern Bering Sea. Harmful Algae 27, 52-59.
688 https://doi.org/10.1016/j.hal.2013.04.006.

689 Natsuike, M., Oikawa, H., Matsuno, K., Yamaguchi, A., Imai, I., 2017b. The physiological
690 adaptations and toxin profiles of the toxic Alexandrium fundyense on the eastern Bering Sea and
691 Chukchi Sea shelves. Harmful Algae 63, 13-22. https://doi.org/10.1016/j.hal.2017.01.001.

692 Nikolopoulos, A., Pickart, R.S., Fratantoni, P.S., Shimada, K., Torres, D.J., Jones, E.P., 2009.
693 The western Arctic boundary current at 152°W: Structure, variability, and transport. Deep-Sea
694 Res. Pt. II 56(17), 1164-1181. https://doi.org/10.1016/j.dsr2.2008.10.014.

695 Pickart, R.S., Moore, G.W.K., Torres, D.J., Fratantoni, P.S., Goldsmith, R.A., Yang, J., 2009.
696 Upwelling on the continental slope of the Alaskan Beaufort Sea: Storms, ice, and oceanographic
697 response. J. Geophys. Res-Oceans 114(C1). https://doi.org/10.1029/2008jc005009.

698 Pickart, R.S., Spall, M.A., Mathis, J.T., 2013. Dynamics of upwelling in the Alaskan Beaufort
699 Sea and associated shelf–basin fluxes. Deep-Sea Res. Pt. I 76, 35-51.
700 http://dx.doi.org/10.1016/j.dsr.2013.01.007.

701 Pickart, R.S., Spall, M.A., Moore, G.W.K., Weingartner, T.J., Woodgate, R.A., Aagaard, K.,
702 Shimada, K., 2011. Upwelling in the Alaskan Beaufort Sea: Atmospheric forcing and local
703 versus non-local response. Prog. Oceanogr. 88(1), 78-100.
704 https://doi.org/10.1016/j.pocean.2010.11.005.

705 Pitcher, G.C., Jiménez, A.B., Kudela, R.M., Reguera, B., 2017. Harmful Algal Blooms in
706 Eastern Boundary Upwelling Systems

707 A GEOHAB Core Research Project. Oceanogr. 30(1), 22-35.
708 https://doi.org/10.5670/oceanog.2017.107.

709 Prud'homme van Reine, W.F., 2017. Report of the Nomenclature Committee for Algae: 16 – On
710 proposals to amend the Code. Taxon 66(1), 197-198. https://doi.org/10.12705/661.18.

711 Schulze, L.M., Pickart, R.S., 2012. Seasonal variation of upwelling in the Alaskan Beaufort Sea:
712 Impact of sea ice cover. J. Geophys. Res-Oceans 117(C6).
713 https://doi.org/10.1029/2012JC007985.

714 Smayda, T.J., Trainer, V.L., 2010. Dinoflagellate blooms in upwelling systems: Seeding,
715 variability, and contrasts with diatom bloom behaviour. Prog. Oceanogr. 85(1), 92-107.
716 https://doi.org/10.1016/j.pocean.2010.02.006.

717 Spall, M.A., 2004. Boundary Currents and Watermass Transformation in Marginal Seas. J. Phys.
718 Oceanogr. 34(5), 1197-1213. https://doi.org/10.1175/1520-
719 0485(2004)034<1197:BCAWTI>2.0.CO;2.

720 Stoeck, T., Bass, D., Nebel, M., Christian, R., Jones, M.D.M., Breiner, H.-W., Richards, T.A.,
721 2010. Multiple marker parallel tag environmental DNA sequencing reveals a highly complex
722 eukaryotic community in marine anoxic water. Mol. Ecol. 19(s1), 21-31.
723 https://doi.org/10.1111/j.1365-294X.2009.04480.x.

724 Tenore, K.R., Alonso-Noval, M., Alvarez-Ossorio, M., Atkinson, L.P., Cabanas, J.M., Cal, R.M.,
725 Campos, H.J., Castillejo, F., Chesney, E.J., Gonzalez, N., Hanson, R.B., McClain, C.R.,
726 Miranda, A., Roman, M.R., Sanchez, J., Santiago, G., Valdes, L., Varela, M., Yoder, J., 1995.
727 Fisheries and oceanography off Galicia, NW Spain: Mesoscale spatial and temporal changes in
728 physical processes and resultant patterns of biological productivity. J. Geophys. Res-Oceans
729 100(C6), 10943-10966. https://doi.org/10.1029/95JC00529.

730 van der Linden, E.C., Le Bars, D., Bintanja, R., Hazeleger, W., 2019. Oceanic heat transport into
731 the Arctic under high and low CO2 forcing. Clim. Dynam. 53(7), 4763-4780.
732 https://doi.org/10.1007/s00382-019-04824-y.

733 Wall, D., 1971. Biological Problems concerning Fossilizable Dinoflagellates. Proc. Ann. Meet.
734 Am. Assoc. Stratigr. Palynol. 2, 1-15. https://doi.org/10.2307/3687273.

735 Wang, D.-Z., 2008. Neurotoxins from Marine Dinoflagellates: A Brief Review. Mar. Drugs 6(2),
736 349-371. https://doi.org/10.3390/md20080016

737 Woodgate, R.A., 2018. Increases in the Pacific inflow to the Arctic from 1990 to 2015, and
738 insights into seasonal trends and driving mechanisms from year-round Bering Strait mooring
739 data. Prog. Oceanogr. 160, 124-154. https://doi.org/10.1016/j.pocean.2017.12.007.

740 Wyatt, T., Jenkinson, I.R., 1997. Notes on Alexandrium population dynamics. J. Plankton Res.
741 19(5), 551-575. https://doi.org/10.1093/plankt/19.5.551.

742 Yarimizu, K., Sildever, S., Hamamoto, Y., Tazawa, S., Oikawa, H., Yamaguchi, H., Basti, L.,
743 Mardones, J.I., Paredes-Mella, J., Nagai, S., 2021. Development of an absolute quantification
744 method for ribosomal RNA gene copy numbers per eukaryotic single cell by digital PCR.
745 Harmful Algae 103, 102008. https://doi.org/10.1016/j.hal.2021.102008.

746

747

Table 1.

753   **Table 2.** P-values from Dunn's post hoc test comparing differences in 18S rRNA relative

754   abundance of *A. catenella* sequencing reads in shelf samples (surface and chl-*a*) between

755   occupations of the transect. ns – not significant.

	A	B	C	D
A	--			
B	0.043	--		
C	0.0015	ns	--	
D	<0.0001	ns	0.040	--

756

757
758   **Figure legends**

759   **Figure 1**

760   Map of the study area, including place names, and schematic circulation of the region. The flow

761   emanating from Barrow Canyon splits, with the eastward-flowing portion forming the Beaufort

762   Shelfbreak Jet. The locations of the repeat transect, the AON mooring, and the test station are

763   marked (see the legend). The bathymetry is from IBCAO v3. The inset shows an enlarged view

764   of the measurement sites used in the study.

765   **Figure 2**

766   Timeseries of the upwelling event. (A) The alongcoast wind speed from the Utqiaġvik weather

767   station and the ERA5 reanalysis. Negative values correspond to winds from the east. The grey

768   bars denote the time periods of the four ship transects occupations. (B) Alongstream velocity,

769   where positive is to the east. (C) Salinity (color) overlain by potential density (contours, kg m^{-3}).

770   The blue dots denote the locations of the MicroCATs on the mooring. (D) Same as (C) except for

771   potential temperature (color).

772   **Figure 3**

773   Vertical sections of potential temperature (color) overlain by potential density (contours, kg m^{-3})

774   for (A) onset of upwelling, (B) during upwelling, and (C, D) after upwelling. Station locations

775   indicated by triangles across the top of the section with blue triangles indicating those at which

776   surface water was collected. While the AON mooring is not on the transect, the location of the

777   mooring with respect to the shelf on the sampled transect is plotted as a blue line for reference

778   with dots indicating the locations of MicroCATs along the mooring profile. The corresponding

779   concentrations of absolute *A. catenella* 28S rRNA gene abundance from surface collected

780   samples are plotted above the sections, with the relative fraction of *A. catenella* 18S rRNA of

781   total eukaryotic phytoplankton (dinoflagellates, diatoms, haptophytes) 18S rRNA indicated by

782   the symbol size. Thresholds that were imaged by FlowCAM were 28S rRNA gene abundance of

783   > 3.92E+09 gc L^{-1} and a relative *A. catenella* 18S rRNA abundance of the total phytoplankton

784   community of > 45%.

785   **Figure 4**

786   Observed relationships between *A. tamarense* 28S gene abundance and other measured variables**.**

787   A) Relationship between relative *A. catenella* 18S rRNA as a fraction of total eukaryotic

788   phytoplankton (dinoflagellates, diatoms, haptophytes)18S rRNA and absolute *A. catenella* 28S

789   rRNA gene abundance; both are on a log scale. B) Relationship plotted between fluorescence

790   and absolute 28S rRNA gene abundance of *A. catenella*; not on a log scale. Samples that had a

791   relative abundance of *A. catenella* above 5% (from 18S analysis) are solid black circles and

792   samples that had a relative abundance below 5% are empty black circles.

Figure 1
Click here to access/download;Figure;Figure1_sch_L_Alb.tif
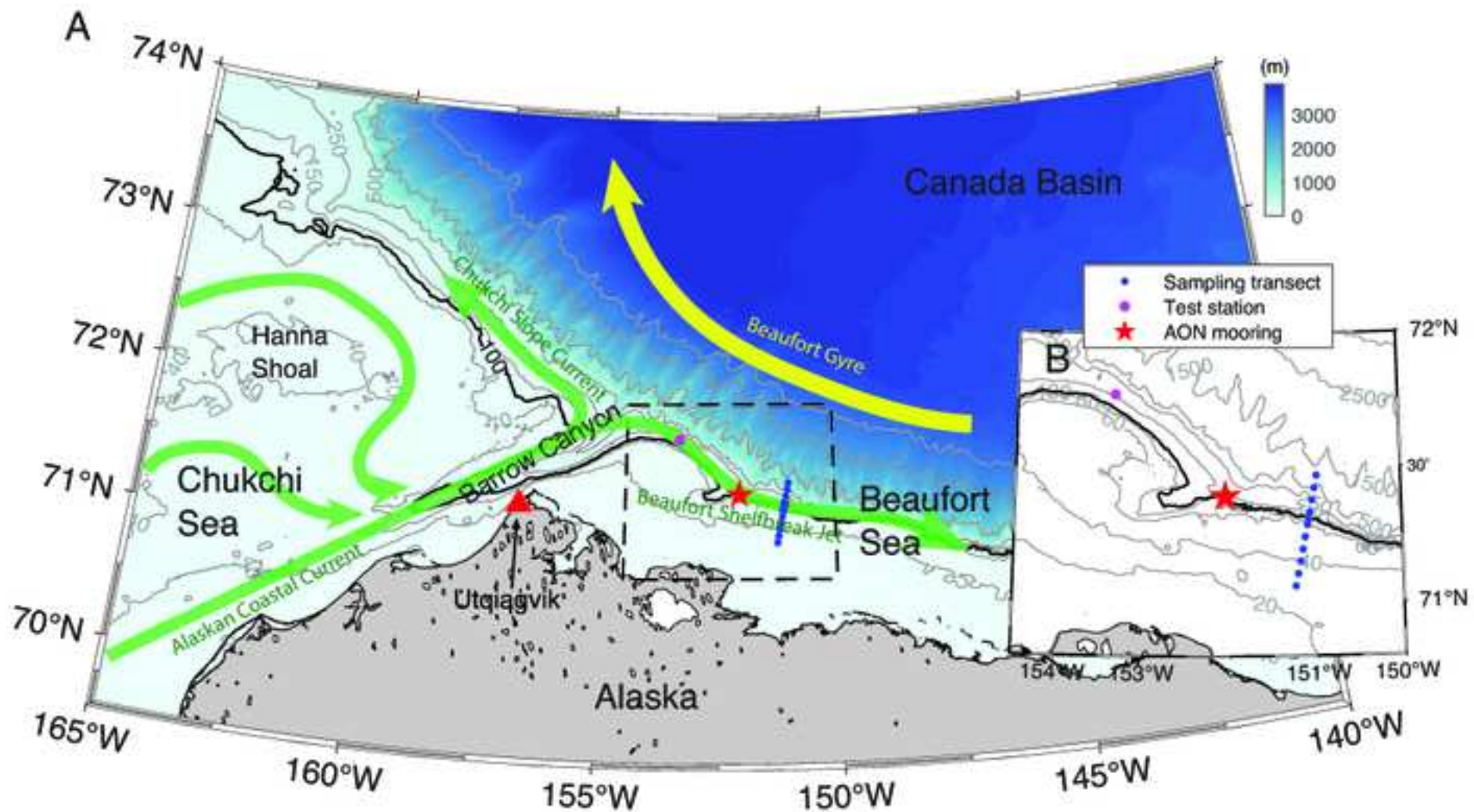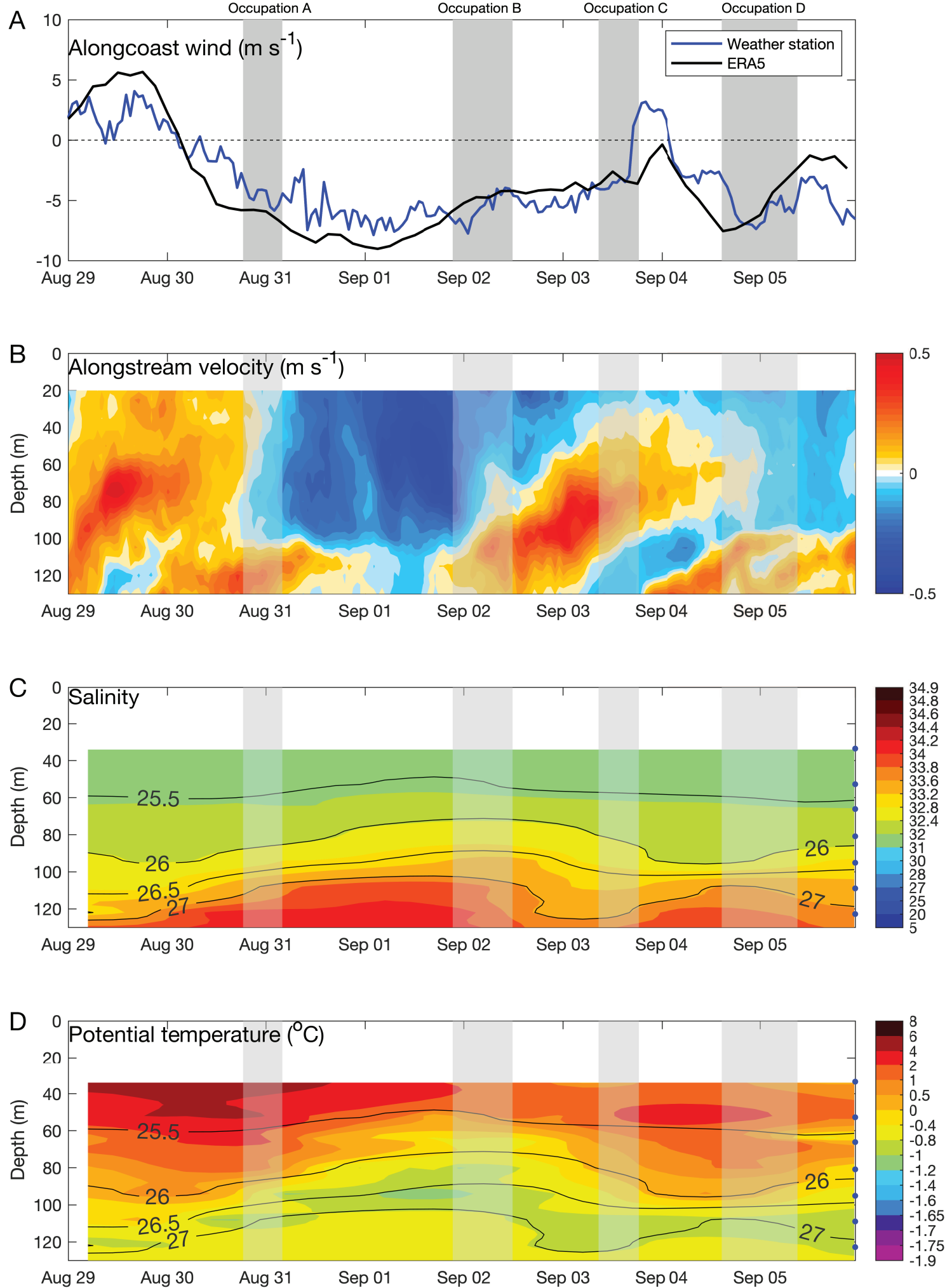
Figure 2

Figure 2

Figure 3
Click here to access/download;Figure;Figure3.eps

Figure 4

Figure 4